ACS Medicinal Chemistry Letters

pubs.acs.org/acsmedchemlett Letter

A New Highly Deuterated [^{18}F]AV-45, [^{18}F]D15FSP, for Imaging β-Amyloid Plaques in the Brain

Hao Xiao, Seok Rye Choi, Ruiyue Zhao, Karl Ploessl, David Alexoff, Lin Zhu, Zhihao Zha, and Hank F. Kung*

Cite This: *ACS Med. Chem. Lett.* 2021, 12, 1086−1092 Read Online

ACCESS | Metrics & More | Article Recommendations | Supporting Information

ABSTRACT: [^{18}F]AV-45 (florbetapir f18, Amyvid) is an FDA-approved PET imaging agent targeting Aβ plaques in the brain for diagnosis of Alzheimer's disease (AD). Its metabolites led to a high background in the brain and large bone uptake of [^{18}F]F$^-$, produced from dealkylation of the PEG chain. To slow down the in vivo metabolism, we report the design, synthesis, and evaluation of a highly deuterated derivative, [^{18}F]D15FSP, and compared it with *N*-methyl-deuterated [^{18}F]D3FSP and nondeuterated [^{18}F]AV-45. D15FSP displayed excellent binding affinity (K_i = 7.52 nM) to Aβ aggregates. In vitro autoradiography of [^{18}F]D15FSP, [^{18}F]D3FSP, and [^{18}F]AV-45 showed excellent binding to Aβ plaques in human AD brain sections. Biodistribution studies displayed lower bone uptake at 120 min for [^{18}F]D15FSP compared to that for [^{18}F]D3FSP and [^{18}F]AV-45 (1.44 vs 4.23 and 4.03%ID/g, respectively). As the highly deuterated [^{18}F]D15FSP displayed excellent Aβ binding affinity, high initial brain penetration, and lower bone retention, it might be suitable for PET imaging in detecting Aβ plaques.

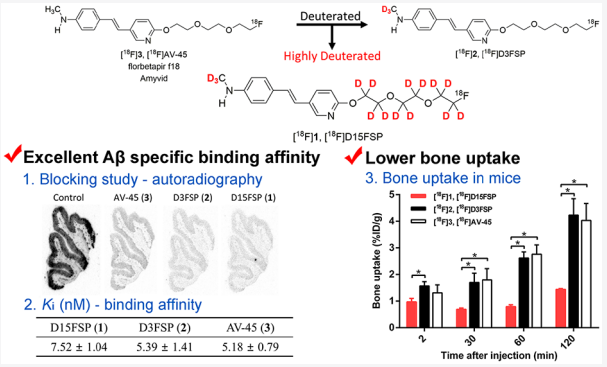

KEYWORDS: *Alzheimer's disease, [^{18}F]AV-45, deuterium, β-amyloid, in vivo metabolism*

Alzheimer's disease (AD) is a common neurodegenerative disorder. It is characterized neuropathologically by the accumulation of β-amyloid protein aggregates (Aβ plaques) and tau protein (tangles) in the brain.[1,2] Positron emission tomography (PET) imaging of Aβ plaques in the brain is a useful tool to define the presence of Aβ plaques, a critical risk factor for AD. A negative scan is highly beneficial as it definitively rules out AD. Therefore, amyloid PET imaging provides specific information on the underlying pathology.[3−5] One of the well-studied PET imaging agents targeting Aβ plaques in the brain is Pittsburgh Compound-B ([^{11}C]PIB)[6,7] (Figure 1). Due to the short physical half-life of ^{11}C ($T_{1/2}$ = 20 min), PIB is not readily available commercially. ^{18}F ($T_{1/2}$ = 110 min)-labeled amyloid imaging agents are attractive for a large-scale patient study and widespread distribution. Three ^{18}F-labeled tracers have been successfully developed and approved by the FDA,[8,9] including [^{18}F]AV-45 (florbetapir f18, Amyvid), [^{18}F]AV-1 (florbetaben f18, Neuraceq), and [^{18}F]FPIB (flutemetamol f18, Vizamyl) (Figure 1). Among them, [^{18}F]AV-45 was the first tracer approved by the FDA for human Aβ imaging.[3,10] Post-mortem studies of AD patients showed that [^{18}F]AV-45 PET imaging prior to the death correlated well with the regional distribution of Aβ plagues in the brain.[10] [^{18}F]AV-45 has been widely accepted as a clinical tool for in vivo visualization and quantification of Aβ plaques in the brain of suspected AD patients. Amyloid PET imaging provides information which could benefit millions of patients who are suffering from this disease.[11]

Previous reports on in vivo metabolism of [^{18}F]AV-45 in mice showed a rapid drop of the plasma concentration after i.v. injection.[12] At 30 min after an intravenous injection, only 30% of the parent compound, [^{18}F]AV-45, remained in the plasma. Comparably, [^{18}F]AV-1 also displayed a rapid in vivo metabolism.[13,14] Due to the close similarity in the chemical structures between [^{18}F]AV-45 and [^{18}F]AV-1 (Figure 1), they exhibited similar in vivo pharmacokinetics and metabolic profiles.[15,16] One of the major metabolites for both tracers resulted from the loss of the fluoropolyethylene glycol (PEG) side chain, which subsequently led to production of [^{18}F]-fluoroethanol and [^{18}F]fluoride. Bone uptake of [^{18}F]fluoride in vivo could serve as a surrogate for measuring in vivo defluorination.[17]

Received: January 26, 2021
Accepted: June 17, 2021
Published: June 21, 2021

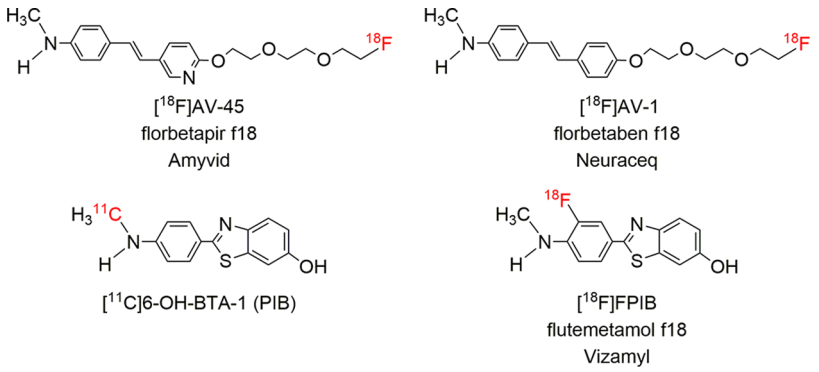

Figure 1. Chemical structures of the four most commonly employed PET imaging agents targeting Aβ plaques in the living human brain.

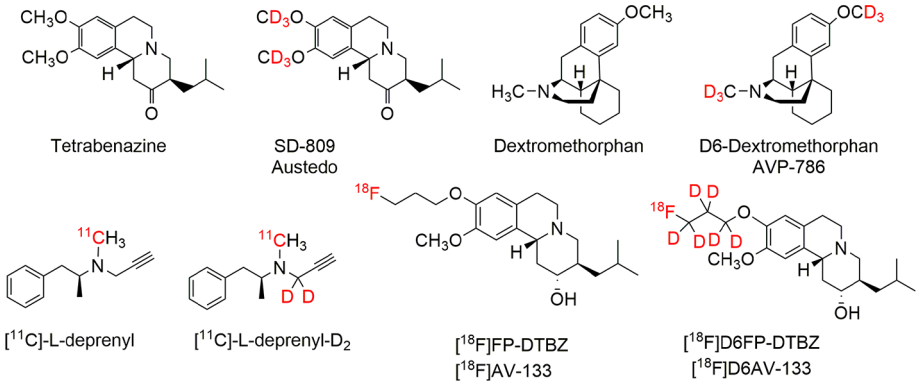

Figure 2. Examples of deuterium substituted drugs and PET imaging agents.

Scheme 1. Synthesis of Nonradioactive D15FSP (1) and Its Precursor (4) for Fluorination

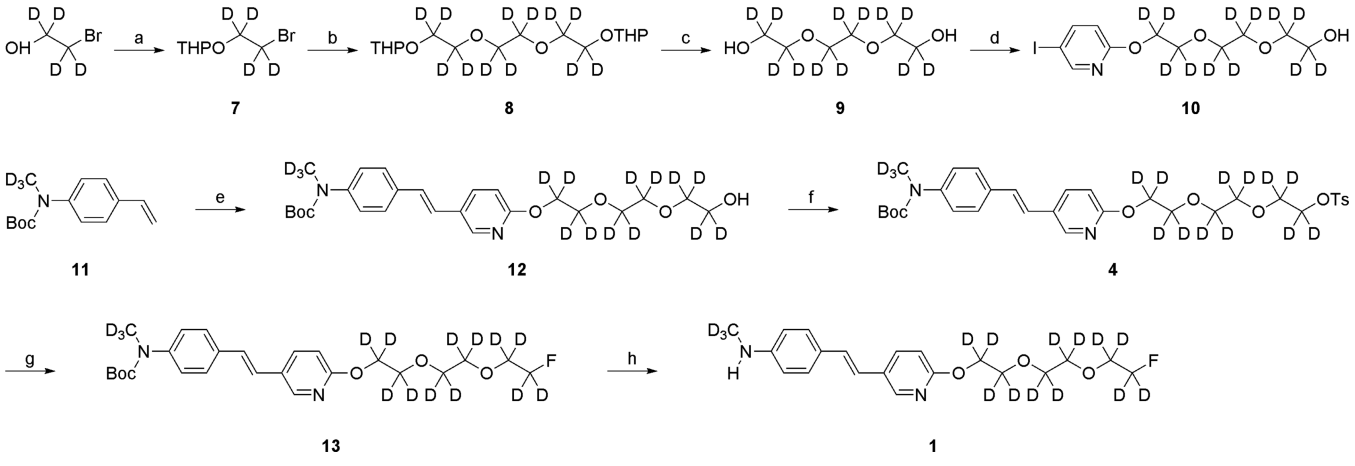

We hypothesized that deuterium substitution for hydrogen on the PEG chain might slow down the suspected in vivo metabolism. The utility of deuterium substitution for hydrogen to alter pharmacokinetics and metabolism in pharmaceuticals is a valuable approach in the toolbox of medicinal chemists.[18−21] In April 2017, the FDA approved deuterated tetrabenazine (SD-809, Austedo) (Figure 2) for the treatment of chorea with Huntington's disease. Dextromethorphan and D6-dextromethorphan (AVP-786) (Figure 2) have received fast track designation by the FDA but have not yet reached regulatory approval.[20,22] Several successful examples of PET imaging agents using deuterium substitution for hydrogen have been reported,[23,24] including [^{11}C]-L-deprenyl-D2[25−27] (instead of [^{11}C]-L-deprenyl) for mapping MAO-B activity in the brain. One recently reported example is the use of a deuterated DTBZ derivative, [^{18}F]D6FP-DTBZ[28,29] (a derivative of [^{18}F]AV-133) (Figure 2) for mapping vesicular monoamine transporter 2 (VMAT2) in the brain. The deuterated [^{18}F]D6FP-DTBZ displayed excellent specific target binding, high regional specific uptake in the striatum of the brain, and a clear advantage in reduction of in vivo bone uptake in rats. To some extent, they all showed different degrees of modified pharmacokinetic and metabolic profiles. Deuterium substitution for hydrogen may also present a beneficial effect by decreasing in vivo defluorination, thereby reducing bone uptake and background activity.[20]

By modifying the in vivo kinetics, this highly deuterated imaging agent, [^{18}F]D15FSP, may lead to an alternative useful

https://doi.org/10.1021/acsmedchemlett.1c00062
ACS Med. Chem. Lett. 2021, 12, 1086−1092

Scheme 2. Preparation of [^{18}F]D15FSP ([^{18}F]1), [^{18}F]D3FSP ([^{18}F]2), and [^{18}F]AV-45 ([^{18}F]3)

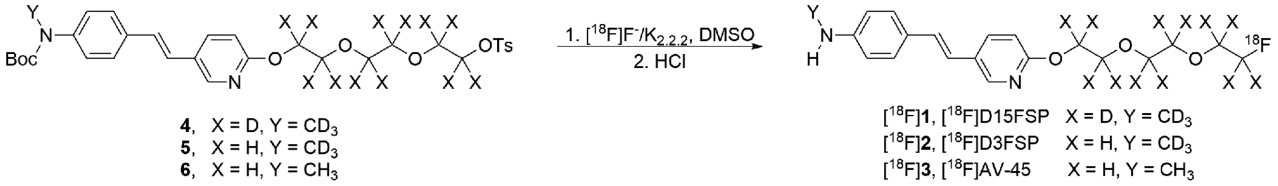

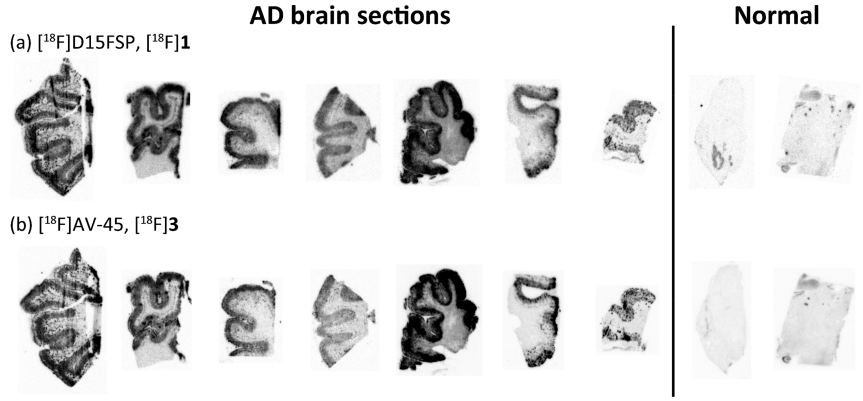

Figure 3. Comparison of in vitro autoradiography images between (a) [^{18}F]D15FSP and (b) [^{18}F]AV-45 on frozen post-mortem brain tissue sections from brain regions of various patients with Alzheimer's disease (seven samples starting on the left) and healthy control (two samples on the right). Both tracers showed consistent and comparable β-amyloid plaque binding.

PET imaging agent targeting amyloid plaques in the brain. We report herein the synthesis and biological evaluation of this potential new imaging agent based on deuterium substitution for hydrogen approach.

Synthesis of the cold standard compound D15FSP (**1**) and its precursor (**4**) for fluorine labeling is shown in Scheme 1. Synthesis and characterization of related compounds are included in the Supporting Information. THP-protected compound **7** was prepared by using D4-2-bromoethanol as the starting material. Subsequent coupling reaction with D4-1,2-dihydroxyethane in the presence of sodium hydride yields predominantly the desired D12-substituted compound **9** in a yield of 41.9%. The PEGylated pyridine **10** was produced by a coupling reaction of compound **9** with 2-chloro-5-iodopyridine, which was followed by the Pd-catalyzed coupling with a vinyl precursor compound **11**. The resulting alcohol **12** was then transformed into a tosylated compound **4** (overall yield 5.0%), which also served as a precursor for radiolabeling with [^{18}F]fluoride. Precursor **4** for fluorination was then reacted with TBAF to give intermediate **13**. The *N*-Boc protecting group of compound **13** was selectively removed by TFA hydrolysis to give the desired final product, D15FSP (**1**), in an overall yield of 2.0%.

Radiolabeling procedures (Scheme 2) were similar to published methods for [^{18}F]AV-45.[12] Precursor **4** was radiolabeled with activated [^{18}F]fluoride with $K_{2.2.2}/K_2CO_3$ in DMSO for 15 min at 110 °C. After being cooled, the protection group was cleaved with 10% aqueous HCl solution at 100 °C for 10 min. The product, [^{18}F]D15FSP, was then purified by semipreparative HPLC. Starting activities used were 945 ± 541 MBq (n = 3), with radiochemical purities of the final product determined to be 96.6 ± 1.7%. Radiochemical yields (decay corrected) were 53.0 ± 7.8% with molar activities (A_m) of 23.0 ± 7.4 GBq/μmol. [^{18}F]D3FSP and [^{18}F]AV-45 were synthesized in a similar manner.[12,17]

The selective and specific binding of [^{18}F]D15FSP to β-amyloid plaques was performed by autoradiography. Adjacent AD brain tissue sections were incubated with [^{18}F]D15FSP or [^{18}F]AV-45 in vitro to compare the tracers' binding to β-amyloid plaques directly. The images of autoradiography (Figure 3) for both [^{18}F]D15FSP and [^{18}F]AV-45 showed very similar results. The β-amyloid plaques in the gray matter labeled by radiotracers are displayed as a darkly speckled band on the edge of the gray matter, while the lightly stained area in the center of the tissue reflects that the white matter (where density of β-amyloid plaques is usually very low) is not labeled by radiotracers specifically.

A blocking study suggested that specific [^{18}F]D15FSP binding to adjacent AD brain sections was blocked by "cold" D15FSP, D3FSP, and AV-45 at the concentration of 5 μM, indicating that they are competing for the same binding sites (Figure 4). The autoradiography studies of [^{18}F]D15FSP and [^{18}F]AV-45 demonstrate that these two agents shared the same selective and specific binding to β-amyloid binding regions of

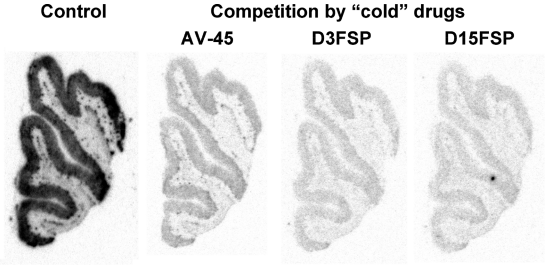

Figure 4. Autoradiography images of adjacent post-mortem AD brain sections using [^{18}F]D15FSP: control and blocking of β-amyloid plaque binding by various "cold" competing drugs—AV-45, D3FSP, or D15FSP. The concentration of competing drugs was 5 μM. Significant reduction of the signal implied that they are competing for the same binding sites.

https://doi.org/10.1021/acsmedchemlett.1c00062
ACS Med. Chem. Lett. 2021, 12, 1086−1092

AD brain, and they showed high specificity in binding to Aβ plaques in the gray matter of these adjacent AD brain sections.

Next, an in vitro binding assay was used to measure affinity to Aβ aggregates in the AD brain tissue homogenates for "cold" D15FSP, D3FSP, and AV-45. The inhibition constants (K_i, nM) of "cold" competing ligands against binding of [^{125}I]-IMPY,[12,30] a known Aβ binding ligand, are presented in Table 1. As expected, the highly deuterated analogue D15FSP displayed excellent binding affinity (K_i = 7.52 ± 1.04 nM). No significant differences among three compounds were observed in binding affinity to amyloid. Their binding patterns and intensity in post-mortem brain tissue sections from AD patients are very similar, which demonstrate high selectivity and specificity of these compounds to β-amyloid plaques.

Table 1. In Vitro Binding Affinity to β-Amyloid Plaques of Human AD Brain Homogenates with [^{125}I]IMPY,[12,30] a Known Aβ Binding Ligand, as the Ligand (K_i, nM, Avg ± SD, n = 4)

competition drugs	D15FSP	D3FSP	AV-45
K_i, nM	7.52 ± 1.04	5.39 ± 1.41	5.18 ± 0.79

Finally, biodistribution studies using normal mice were performed for [^{18}F]D15FSP (Supporting Information). The results were compared with previously reported for [^{18}F]AV-45 and [^{18}F]D3FSP.[12,17] After an i.v. injection into the tail vein of normal mice, all three tracers, [^{18}F]AV-45, [^{18}F]D3FSP, and [^{18}F]D15FSP, showed good initial brain penetration and washout from mice brain, as shown in Table 2. [^{18}F]D15FSP entered the brain and reached 6% injected dose per gram (% ID/g) within 2 min. Then, the activity in the brain cleared rapidly and dropped to 1.3%ID/g by 30 min. These tracers showed high initial uptake in the brain and washed out rapidly due to absence of β-amyloid deposits in a normal mouse brain. In Alzheimer's patients, [^{18}F]AV-45 displayed higher retention in the brain due to presence of Aβ plaques.

The two deuterium-substituted tracers, [^{18}F]D15FSP and [^{18}F]D3FSP, showed lower residual activity in the brain (at 60 and 120 min), which might possibly suggest an improved image contrast for amyloid plaque in AD patients. Results for [^{18}F]D15FSP showed the lowest residual retention of activity in the brain at 120 min post-i.v. injection. Based on the initial uptake at 2 min, the kinetics of brain uptake and washout of these three tracers at 30, 60, and 120 min were normalized (Figure 5). [^{18}F]D15FSP showed a lower residual brain retention as compared to those of [^{18}F]AV-45 and [^{18}F]D3FSP. Although the statistical significance is low (low number of mice (n = 3) for each time point and the absence of target amyloid in the normal brain), this observation suggests that [^{18}F]D15FSP might have improved metabolic stability, which results in overall lower activity in the normal brain. However, more data are needed to confirm this.

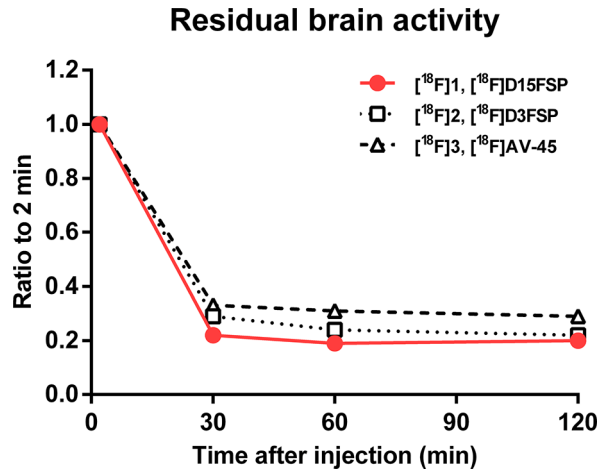

Figure 5. Ratio of brain activity in normal mice at 30, 60, and 120 min vs 2 min of [^{18}F]D15FSP and [^{18}F]D3FSP and [^{18}F]AV-45.

Biodistribution studies in mice showed that [^{18}F]D15FSP and [^{18}F]D3FSP displayed lower residual blood activity in 2 h postinjection, which might be beneficial to improve the image contrast for amyloid plaque detection when tested in AD patients with Aβ deposition in the brain (Table 2).

The biodistribution results in normal mice showed that [^{18}F]D15FSP, [^{18}F]D3FSP, and [^{18}F]AV-45 displayed similar uptake in most organs, except for the bone uptake. The bone uptake of [^{18}F]AV-45, [^{18}F]D3FSP, and [^{18}F]D15FSP at 2 and 120 min were 1.31/4.04, 1.57/4.23, and 0.97/1.44%ID/g, respectively (Figure 6). This shows a significant drop in bone uptake of [^{18}F]D15FSP, indicating a statistically significant reduction of defluorination. However, it appeared that there were no significant differences between the bone uptake between [^{18}F]D3FSP and [^{18}F]AV-45 (Figure 6). Seemingly, the lower bone uptake is prominent only for the highly deuterated [^{18}F]D15FSP. It is reasonable to speculate that the deuterium substitution on the fluoro-PEG side chain leads to a decrease in in vivo defluorination.

It was reported that N-demethylation is one of the major pathways of metabolism in [^{18}F]AV-45 and [^{18}F]AV-1.[12,17] Previous research on in vitro metabolism of [^{18}F]AV-45 in rat liver microsomes also suggested that the N-demethylated metabolite of [^{18}F]AV-45 was further degraded by cleavage of

Table 2. Brain and Blood Uptake of [^{18}F]D15FSP,[a], [^{18}F]D3FSP,[b] and [^{18}F]AV-45[b] in CD-1 Mice (%ID/g, Avg ± SD, n = 3−6)

		time after injection (min)			
organ	tracer	2	30	60	120
brain	[^{18}F]D15FSP	5.99 ± 0.14	1.30 ± 0.19	1.11 ± 0.03	1.18 ± 0.11
	[^{18}F]D3FSP	5.69 ± 0.31	1.66 ± 0.20	1.37 ± 0.13	1.24 ± 0.06
	[^{18}F]AV-45	4.77 ± 0.61	1.59 ± 0.16	1.46 ± 0.16	1.38 ± 0.18
blood	[^{18}F]D15FSP	2.21 ± 0.16	2.16 ± 0.16	1.98 ± 0.24	1.51 ± 0.28
	[^{18}F]D3FSP	2.14 ± 0.12	1.94 ± 0.41	1.88 ± 0.17	1.47 ± 0.19
	[^{18}F]AV-45	2.49 ± 0.29	2.71 ± 0.38	2.17 ± 0.38	1.74 ± 0.31

[a]Detailed data for biodistribution of [^{18}F]D15FSP are presented in Supporting Information (Table S1). [b]Averaged values for [^{18}F]D3FSP and [^{18}F]AV-45 were from previously reported data[12,17] and other in-house data.

https://doi.org/10.1021/acsmedchemlett.1c00062
ACS Med. Chem. Lett. 2021, 12, 1086−1092

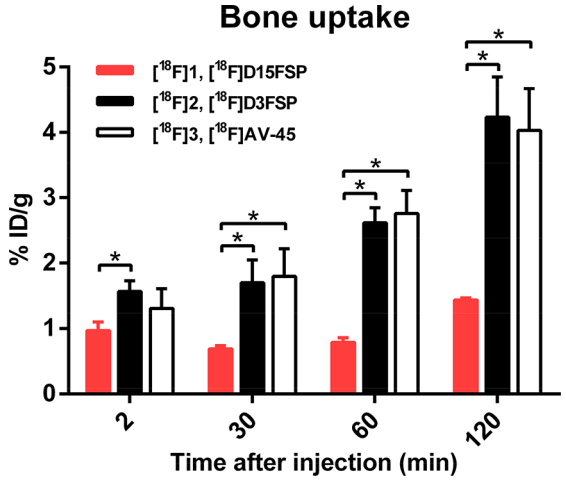

Figure 6. Comparison of bone uptake among [^{18}F]D15FSP, [^{18}F]D3FSP, and [^{18}F]AV-45. In vivo biodistribution of [^{18}F]D15FSP showed a clearly distinctive lower bone uptake, suggesting a lower amount of free fluoride metabolite than that with the other two compounds, [^{18}F]D3FSP and [^{18}F]AV-45. *$p < 0.05$ was considered a statistically significant difference by *t*-test.

the PEG side chain.[31] [^{18}F]fluoroethanol might serve as one of the major metabolites of [^{18}F]AV-45 through the O-dealkylation pathway. Subsequently, it would then be oxidized to [^{18}F]fluoroacetaldehyde, which was further metabolized to [^{18}F]fluoroacetate and trapped inside the cell by the form of [^{18}F]fluoroacetyl-CoA.[32] As a result, [^{18}F]fluoroethanol showed a high and prolonged retention in the brain and blood.[33,34] In the O-dealkylation reaction, cytochrome P450 may catalyze hydroxylation of a C−H bond α to the oxygen atom, followed by an oxidation reaction leading to the removal of the ether.[35] As C−D bonds are slightly shorter and more stable than C−H bonds, deuterium substitution for hydrogen would in theory show slower kinetics in breaking of C−D bond in the O-dealkylation,[20] thereby leading to a better stability of [^{18}F]D15FSP, as compared to that of [^{18}F]D3FSP and [^{18}F]AV-45. As a consequence, deuterium substitution for hydrogen might reduce the level of [^{18}F]fluoroethanol and the next level metabolite, [^{18}F]2-fluoroacetylaldehyde in the blood circulation, which cross the blood−brain barrier and lead to higher background in the brain.[33,34] The subsequent metabolite is [^{18}F]F$^-$, which is reflected in higher bone uptake. This might be a plausible explanation on why [^{18}F]D15FSP displayed more rapid blood clearance, which might lower residual activity in the brain. In addition, [^{18}F]D15FSP showed significantly lower bone uptake compared to those of [^{18}F]D3FSP and [^{18}F]AV-45, suggesting less defluorination as explained above. At this moment, it is unknown if the highly deuterated [^{18}F]D15FSP would be useful when applied in AD patients. Results for modifying in vivo metabolism by the heavily deuterated alternative agent should be worthy of evaluation in humans in the future.

Human radiation dosimetry was estimated based on the biodistribution of [^{18}F]D15FSP after i.v. injection in normal male mice. The organs that were estimated to receive high doses of [^{18}F]D15FSP were kidneys, liver, and intestines. The effective estimated human dose (ED) of [^{18}F]D15FSP was calculated as 18.9 μSv/MBq for a human male. As shown in Table 3, the estimated radiation dose of [^{18}F]D15FSP is very comparable to those of other amyloid imaging agents and supports further investigation of [^{18}F]D15FSP in humans.

Table 3. Comparison of ED Estimates for [^{18}F]D15FSP with Other Amyloid Radiopharmaceuticals

tracer	subject	ED (μSv/MBq)
[^{18}F]D15FSP	male mice	19.5
florbetapir ([^{18}F]AV-45)	3 males and 6 females human data	18.6
flutemetamol ([^{18}F] GE067)	5 males and 1 female human data	33.8
florbetaben ([^{18}FAV-1)	2 males and 1 female human data	14.7
[^{18}F]FDG		19.0
[^{11}C]PIB	3 males and 3 females human data	5.3

Since there are already three FDA-approved Aβ plaque imaging agents available commercially, one may argue that there is no need for further research in this area. However, analysis of amyloid/PET images produced by [^{18}F]AV-45 still poses challenging problems. In many cases, it is difficult to visually separate images between the AD and mild-cognitive impairment patients from those of normal aging subjects.[36] Interpretation of the brain images requires prior training for nuclear medicine physicians as mandated by the FDA. This is likely due to the fact that the regional distribution of signal density (reflecting specific Aβ plaque binding) in the gray areas of the cortex are very close to the white matter in the interior of the brain. Signals in the white matter represent nonspecific binding, as post-mortem pathological studies of AD brain white matter showed very low Aβ plaque density.[10,37] There remains a need to improve the diagnostic interpretation by increasing the signal of specific binding against noise. Deuterated imaging agents producing lower in vivo metabolites might be a suitable approach to enhance the signal-to-noise ratios in the brain. Though our results have several limitations such as a small number of mice, mice lacking in target amyloid, species and individual differences in CYP enzyme activity, etc., they suggest a small step in addressing this critical issue in this field.

In conclusion, highly deuterated [^{18}F]D15FSP is a potential β-amyloid targeting imaging agent. Preliminary studies suggested that [^{18}F]D15FSP is selective in binding to Aβ aggregates with high affinity. In vivo studies in mice showed excellent brain penetration, faster clearance from the normal brain, and a lower bone uptake as compared to that of nondeuterated [^{18}F]AV-45. The improved properties observed for [^{18}F]D15FSP suggest that it might be a suitable candidate as a new Aβ imaging agent to assist the diagnosis of Alzheimer's disease. Estimated dosimetry for [^{18}F]D15FSP suggests ED comparable to that of other radiopharmaceuticals, making it a suitable candidate for further development as a new amyloid imaging agent.

Drs. Zha, Choi, Ploessl, Alexoff and Kung are inventors of a patent, in which [^{18}F]D15FSP was part of the claims. Five Eleven Pharma Inc. holds the patent rights for D15FSP and related technology.[38] All protocols requiring the use of mice were reviewed and approved by the Institutional Animal Care and Use Committee (University of Pennsylvania).

https://doi.org/10.1021/acsmedchemlett.1c00062
ACS Med. Chem. Lett. 2021, 12, 1086−1092

■ ASSOCIATED CONTENT

Supporting Information

The Supporting Information is available free of charge at https://pubs.acs.org/doi/10.1021/acsmedchemlett.1c00062.

Experimental procedure details on the synthesis of compounds, HRMS and NMR spectral data, in vitro binding assays, in vitro autoradiography studies, animal biodistribution and estimated dosimetry data (PDF)

■ AUTHOR INFORMATION

Corresponding Author

Hank F. Kung − *Five Eleven Pharma Inc., Philadelphia, Pennsylvania 19104, United States; Department of Radiology, University of Pennsylvania, Philadelphia, Pennsylvania 19104, United States;* orcid.org/0000-0003-3254-8049; Email: kunghf@gmail.com

Authors

Hao Xiao − *Beijing Institute of Brain Disorders, Laboratory of Brain Disorders, Ministry of Science and Technology, Collaborative Innovation Center for Brain Disorders, Capital Medical University, Beijing 100069, China; Department of Radiology, University of Pennsylvania, Philadelphia, Pennsylvania 19104, United States*

Seok Rye Choi − *Five Eleven Pharma Inc., Philadelphia, Pennsylvania 19104, United States*

Ruiyue Zhao − *Department of Radiology, University of Pennsylvania, Philadelphia, Pennsylvania 19104, United States; Key Laboratory of Radiopharmaceuticals, Ministry of Education, College of Chemistry, Beijing Normal University, Beijing 100875, China*

Karl Ploessl − *Five Eleven Pharma Inc., Philadelphia, Pennsylvania 19104, United States;* orcid.org/0000-0001-7896-5900

David Alexoff − *Five Eleven Pharma Inc., Philadelphia, Pennsylvania 19104, United States*

Lin Zhu − *Key Laboratory of Radiopharmaceuticals, Ministry of Education, College of Chemistry, Beijing Normal University, Beijing 100875, China;* orcid.org/0000-0001-9530-8531

Zhihao Zha − *Five Eleven Pharma Inc., Philadelphia, Pennsylvania 19104, United States*

Complete contact information is available at: https://pubs.acs.org/10.1021/acsmedchemlett.1c00062

Notes

The authors declare no competing financial interest.

■ ACKNOWLEDGMENTS

The authors thank Dr. William Eckelman for insightful discussion and suggestions.

■ ABBREVIATIONS

AD, Alzheimer's disease; PEG, polyethyleneglycol; PET, positron emission tomography; VMAT2, vesicular monoamine transporter 2; TFA, trifluoroacetic acid; THP, tetrahydropyran; DHP, 3,4-dihydropyran; PPTS, pyridinium *p*-toluenesulfonate; DMF, dimethylformamide; DMAP, 4-dimethylaminopyridine; DCM, dichloromethane; DMSO, dimethyl sulfoxide; TBAF, tetra-n-butylammonium fluoride; A_m, molar activity; ED, effective estimated human dose; Sv, sievert; Bq, becquerel

■ REFERENCES

(1) Selkoe, D. J.; Hardy, J. The amyloid hypothesis of Alzheimer's disease at 25 years. *EMBO Mol. Med.* **2016**, *8* (6), 595−608.

(2) Jack, C. R.; Therneau, T. M.; Weigand, S. D.; Wiste, H. J.; Knopman, D. S.; Vemuri, P.; Lowe, V. J.; Mielke, M. M.; Roberts, R. O.; Machulda, M. M.; Graff-Radford, J.; Jones, D. T.; Schwarz, C. G.; Gunter, J. L.; Senjem, M. L.; Rocca, W. A.; Petersen, R. C. Prevalence of Biologically vs Clinically Defined Alzheimer Spectrum Entities Using the National Institute on Aging-Alzheimer's Association Research Framework. *JAMA Neurol* **2019**, *76*, 1174.

(3) Barthel, H. Switching on Brain PET to Light Up Amyloid Pathology In Vivo. *J. Nucl. Med.* **2020**, *61*, 227s−228s.

(4) Mallik, A.; Drzezga, A.; Minoshima, S. Clinical Amyloid Imaging. *Semin. Nucl. Med.* **2017**, *47* (1), 31−43.

(5) Jack, C. R.; Bennett, D. A.; Blennow, K.; Carrillo, M. C.; Dunn, B.; Haeberlein, S. B.; Holtzman, D. M.; Jagust, W.; Jessen, F.; Karlawish, J.; Liu, E.; Molinuevo, J. L.; Montine, T.; Phelps, C.; Rankin, K. P.; Rowe, C. C.; Scheltens, P.; Siemers, E.; Snyder, H. M.; Sperling, R.; Elliott, C.; Masliah, E.; Ryan, L.; Silverberg, N. NIA-AA Research Framework: Toward a biological definition of Alzheimer's disease. *Alzheimer's Dementia* **2018**, *14* (4), 535−562.

(6) Klunk, W. E.; Engler, H.; Nordberg, A.; Wang, Y.; Blomqvist, G.; Holt, D. P.; Bergstrom, M.; Savitcheva, I.; Huang, G.-f.; Estrada, S.; Ausen, B.; Debnath, M. L.; Barletta, J.; Price, J. C.; Sandell, J.; Lopresti, B. J.; Wall, A.; Koivisto, P.; Antoni, G.; Mathis, C. A.; Langstrom, B. Imaging Brain Amyloid in Alzheimer's Disease with Pittsburgh Compound-B. *Ann. Neurol.* **2004**, *55* (3), 306−319.

(7) Mathis, C. A.; Lopresti, B. J.; Ikonomovic, M. D.; Klunk, W. E. Small-molecule PET Tracers for Imaging Proteinopathies. *Semin. Nucl. Med.* **2017**, *47* (5), 553−575.

(8) Kung, H. The *β*-amyloid hypothesis in Alzheimer's disease: Seeing is believing. *ACS Med. Chem. Lett.* **2012**, *3*, 265−267.

(9) Villemagne, V. L.; Dore, V.; Bourgeat, P.; Burnham, S. C.; Laws, S.; Salvado, O.; Masters, C. L.; Rowe, C. C. Abeta-amyloid and Tau Imaging in Dementia. *Semin. Nucl. Med.* **2017**, *47* (1), 75−88.

(10) Clark, C. M.; Schneider, J. A.; Bedell, B. J.; Beach, T. G.; Bilker, W. B.; Mintun, M. A.; Pontecorvo, M. J.; Hefti, F.; Carpenter, A. P.; Flitter, M. L.; Krautkramer, M. J.; Kung, H. F.; Coleman, R. E.; Doraiswamy, P. M.; Fleisher, A. S.; Sabbagh, M. N.; Sadowsky, C. H.; Reiman, E. P.; Zehntner, S. P.; Skovronsky, D. M. Use of florbetapir-PET for imaging beta-amyloid pathology. *JAMA* **2011**, *305* (3), 275−83.

(11) Jagust, W. Imaging the evolution and pathophysiology of Alzheimer disease. *Nat. Rev. Neurosci.* **2018**, *19* (11), 687−700.

(12) Choi, S.; Golding, G.; Zhuang, Z.; Zhang, W.; Lim, N.; Hefti, F.; Benedum, T.; Kilbourn, M.; Skovronsky, D.; Kung, H. Preclinical properties of ^{18}F-AV-45: a PET agent for A*β* plaques in the brain. *J. Nucl. Med.* **2009**, *50*, 1887−1894.

(13) Patt, M.; Schildan, A.; Barthel, H.; Becker, G.; Schultze-Mosgau, M. H.; Rohde, B.; Reininger, C.; Sabri, O. Metabolite analysis of [^{18}F]Florbetaben (BAY 94−9172) in human subjects: a substudy within a proof of mechanism clinical trial. *J. Radioanal. Nucl. Chem.* **2010**, *284* (3), 557−562.

(14) Rowe, C.; Ackerman, U.; Browne, W.; Mulligan, R.; Pike, K.; O'Keefe, G.; Tochon-Danguy, H.; Chan, G.; Berlangieri, S.; Jones, G.; Dickinson-Rowe, K.; Kung, H.; Zhang, W.; Kung, M.; Skovronsky, D.; Dyrks, T.; Holl, G.; Krause, S.; Friebe, M.; Lehman, L.; Lindemann, S.; Dinkelborg, L.; Masters, C.; Villemagne, V. Imaging of amyloid beta in Alzheimer's disease with ^{18}F-BAY94−9172, a novel PET tracer: proof of mechanism. *Lancet Neurol.* **2008**, *7* (2), 129−35.

(15) FDA. Amyvid (Florbetapir F18 Injection); https://www.accessdata.fda.gov/drugsatfda_docs/nda/2012/202008_Florbetapir_Orig1s000TOC.cfm, 2012 (accessed June 18, 2021).

(16) EMA. Neuraceq florbetaben (18F); https://www.ema.europa.eu/documents/assessment-report/neuraceq-epar-public-assessment-report_en.pdf, 2014 (accessed June 18, 2021).

(17) Zha, Z.; Ploessl, K.; Choi, S. R.; Alexoff, D.; Kung, H. F. Preclinical evaluation of [^{18}F]D3FSP, deuterated AV-45, for imaging of *β*-amyloid in the brain. *Nucl. Med. Biol.* **2021**, *92*, 97.

(18) Russak, E. M.; Bednarczyk, E. M. Impact of deuterium substitution on the pharmacokinetics of pharmaceuticals. *Ann. Pharmacother.* **2019**, *53* (2), 211−216.
(19) Howland, R. H. Deuterated Drugs. *J. Psychosoc. Nurs. Ment. Health Serv.* **2015**, *53* (9), 13−16.
(20) Pirali, T.; Serafini, M.; Cargnin, S.; Genazzani, A. A. Applications of deuterium in medicinal chemistry. *J. Med. Chem.* **2019**, *62* (11), 5276−5297.
(21) Gant, T. G. Using deuterium in drug discovery: leaving the label in the drug. *J. Med. Chem.* **2014**, *57* (9), 3595−611.
(22) Tung, R. D. Deuterium medicinal chemistry comes of age. *Future Med. Chem.* **2016**, *8* (5), 491−4.
(23) Kuchar, M.; Mamat, C. Methods to Increase the Metabolic Stability of ^{18}F-Radiotracers. *Molecules* **2015**, *20* (9), 16186−220.
(24) Guengerich, F. P. Kinetic Deuterium Isotope Effects in Cytochrome P450 Reactions. *Methods Enzymol.* **2017**, *596*, 217−238.
(25) Fowler, J. S.; Wang, G. J.; Logan, J.; Xie, S.; Volkow, N. D.; MacGregor, R. R.; Schlyer, D. J.; Pappas, N.; Alexoff, D. L.; Patlak, C.; Wolf, A. P. Selective reduction of radiotracer trapping by deuterium substitution: comparison of carbon-11-L-deprenyl and carbon-11-deprenyl-D_2 for MAO B mapping. *J. Nucl. Med.* **1995**, *36* (7), 1255−1262.
(26) Logan, J.; Fowler, J. S.; Volkow, N. D.; Wang, G. J.; MacGregor, R. R.; Shea, C. Reproducibility of repeated measures of deuterium substituted [^{11}C]L-deprenyl ([^{11}C]L-deprenyl-D2) binding in the human brain. *Nucl. Med. Biol.* **2000**, *27* (1), 43−9.
(27) Arakawa, R.; Stenkrona, P.; Takano, A.; Nag, S.; Maior, R. S.; Halldin, C. Test-retest reproducibility of [^{11}C]-L-deprenyl-D2 binding to MAO-B in the human brain. *EJNMMI Res.* **2017**, *7* (1), 54.
(28) Liu, F.; Choi, S. R.; Zha, Z.; Ploessl, K.; Zhu, L.; Kung, H. F. Deuterated ^{18}F-9-O-hexadeutero-3-fluoropropoxyl-(+)-dihydrotetrabenazine (D6-FP-(+)-DTBZ): A vesicular monoamine transporter 2 (VMAT2) imaging agent. *Nucl. Med. Biol.* **2018**, *57*, 42−49.
(29) Zhao, R.; Zha, Z.; Yao, X.; Ploessl, K.; Choi, S. R.; Liu, F.; Zhu, L.; Kung, H. F. VMAT2 imaging agent, D6-[^{18}F]FP-(+)-DTBZ: Improved radiosynthesis, purification by solid-phase extraction and characterization. *Nucl. Med. Biol.* **2019**, *72*−*73*, 26−35.
(30) Kung, M.-P.; Hou, C.; Zhuang, Z.-P.; Zhang, B.; Skovronsky, D.; Trojanowski, J. Q; Lee, V. M.-Y; Kung, H. F IMPY: An improved thioflavin-T derivative for in vivo Labeling of b-amyloid plaques. *Brain Res.* **2002**, *956* (2), 202−210.
(31) Yin, W.; Zhou, X.; Qiao, J.; Zhu, L. Study the pharmacokinetics of AV-45 in rat plasma and metabolism in liver microsomes by ultra-performance liquid chromatography with mass spectrometry. *Biomed. Chromatogr.* **2012**, *26* (5), 666−671.
(32) Tewson, T. J.; Welch, M. J. Preparation and preliminary biodistribution of ″no carrier added″ fluorine1−8 fluoroethanol. *J. Nucl. Med.* **1980**, *21* (6), 559−564.
(33) Pan, J.; Pourghiasian, M.; Hundal, N.; Lau, J.; Bénard, F.; Dedhar, S.; Lin, K. S. 2-[^{18}F]fluoroethanol and 3-[^{18}F]fluoropropanol: facile preparation, biodistribution in mice, and their application as nucleophiles in the synthesis of [^{18}F]fluoroalkyl aryl ester and ether PET tracers. *Nucl. Med. Biol.* **2013**, *40* (6), 850−7.
(34) Zoghbi, S. S.; Shetty, H. U.; Ichise, M.; Fujita, M.; Imaizumi, M.; Liow, J.; Shah, J.; Musachio, J. L.; Pike, V. W.; Innis, R. B. PET imaging of the dopamine transporter with ^{18}F-FECNT: a polar radiometabolite confounds brain radioligand measurements. *J. Nucl. Med.* **2006**, *47* (3), 520−527.
(35) Silverman, R. B.; Holladay, M. W., Eds. Chapter 8 - Drug Metabolism. In *The Organic Chemistry of Drug Design and Drug Action*, 3rd ed.; Academic Press: Boston, MA, 2014; pp 357−422.
(36) Johnson, K. A.; Sperling, R. A.; Gidicsin, C. M.; Carmasin, J. S.; Maye, J. E.; Coleman, R. E.; Reiman, E. M.; Sabbagh, M. N.; Sadowsky, C. H.; Fleisher, A. S.; Murali Doraiswamy, P.; Carpenter, A. P.; Clark, C. M.; Joshi, A. D.; Lu, M.; Grundman, M.; Mintun, M. A.; Pontecorvo, M. J.; Skovronsky, D. M. Florbetapir (F18-AV-45) PET to assess amyloid burden in Alzheimer's disease dementia, mild cognitive impairment, and normal aging. *Alzheimer's Dementia* **2013**, *9* (S5), S72−83.
(37) Braak, H.; Braak, E. Neuropathological stageing of Alzheimer-related changes. *Acta Neuropathol.* **1991**, *82* (4), 239−59.
(38) Wu, Z.; Zha, Z.; Liu, F.; Ploessl, K.; Choi, S. R.; Kung, H. F. Novel deuterium substituted Positron Emission Tomography (PET) imaging agents and their pharmacological application. USPTO Appl. US 2020/0230263 A1, 2020.

https://doi.org/10.1021/acsmedchemlett.1c00062
ACS Med. Chem. Lett. 2021, 12, 1086−1092